Applied Mathematics & Information Sciences
An International Journal

http://dx.doi.org/10.18576/amis/190310

Mathematical Modeling and Analysis of Stress Transfer Mechanisms in Stone Column-Supported Foundations under Seismic Loading

Mohammed Y. Fattah[1], Makki K. M. Al-Recaby[1], Mohamed Hafez[2,], Ann M. Raheem[1], Moustafa Magdy[3], Mostafa S. Omar[4], and Mohammad Mohie Eldin [5]*

[1] Civil Engineering Department, Faculty of Engineering, University of Technology, Baghdad, Iraq
[2] Civil Engineering Department, FEQS- INTI-IU-Nilai- Malaysia
[3] SIC, Soil Improvement Contracting Company, Dammam-Saudi Arabia
[4] Civil Engineering Department, Faculty of Engineering, Damanhour University, Behira, Egypt
[5] Civil Engineering Department, Faculty of Engineering, Beni Suef University, Beni Suef, Egypt

Received: 7 Aug. 2024, Revised: 21 Sep. 2024, Accepted: 7 Oct. 2024.
Published online: 1 Feb. 2025.

Abstract: The performance of stone columns in enhancing the stability of structures subjected to seismic loads has significant implications for soil improvement in soft clay soils. This research presents a computational and experimental analysis of stress transfer mechanisms in stone column-supported foundations under dynamic seismic loading. A series of mathematical models were developed to simulate stress distribution and displacement patterns within standard and geogrid-encased stone columns (OSC and GESC), incorporating varying shear strengths of clay soils and seismic frequencies. The finite element method (FEM) was employed to validate shaking box model experiments, with 18 models tested across dynamic loading scenarios. Key findings include the influence of frequency and undrained shear strength on lateral stress values and the enhanced resistance offered by geogrid-encased columns. The study further illustrates that stress values at half the depth of the stone column are consistently higher than those at one-third of the depth, corroborating analytical predictions. The integration of experimental data with mathematical analysis provides a robust framework for optimizing stone column design in earthquake-prone regions.

Keywords: Stone column, mathematical modeling, finite element analysis, seismic loading, stress distribution, dynamic systems.

1. Introduction

To increase the bearing capacity of unstable terrain and lessen the settling of buildings constructed on it, stone columns are frequently utilized. By boosting strength, lowering the pressure of soft and weak soils, speeding up the consolidation process, and lowering the soil's propensity for liquefaction, stone columns improve and stabilize the soil. Its primary application stabilizes soft soil types, including silts, soft clays, and silty sands.

The friction and cohesiveness of the stone mass, the friction of the soil around the column, the elasticity or hardness of the foundation that transfers pressure to the improved ground, and the volume of lateral pressure around the soil mass and on both sides of the stone column as a result of the interaction between the various components in the system all contribute to the strength of the bearing of the stone column.

The negative ground pressure resulting from the stone column's bulging and its improved resistance to lateral deformation under additional weight determines the stone column's axial capacity. Many researchers first proposed the theory of load transfer, estimating the final bearing capacity and predicting the stability of the stone column [1].

It is unclear how frequently loading affects the behaviour of soft clay. According to some published research, when the frequency of cyclic loading decreases, there is an increase in both the accumulated pore pressure and the shear strain caused by the loading [2, 3]. The stress level on the surrounding soil will reduce due to the stone column's presence, increasing the overall load carrying capability [4, 5, 6].

Mok et al. [7] used a cross-hole test based on S-wave to examine the deformation of a stone column and verify its integrity. A primary distinction is the application of S-wave, which is typically quantified using an S-wave recorder. The other important point is that recalculating the column dimensions requires knowing the velocity of the s-wave of the column aggregation (V a profile). The angle of

*Corresponding author e-mail: mohdahmed.hafez@newinti.edu.my

internal friction and the earth pressure coefficient at the rest of the column aggregates can be used to examine velocity records. Luckily, the ambiguity in the velocity record makes estimating the column diameter extremely challenging. The technique can help detect bottleneck defects and defects like gourd in the shape of the stone column.

Ashour [8] studied the behavior of stone columns when exposed to cyclic loading. The soil was bred to generate harsh sandy pores. The effect of cyclic pressures and loading frequency on permanent deformation was examined. It was found that the dynamic pressure on the soil threshold for cyclical loading increases with the provision of stone columns.

Three-dimensional (3-D) Finite Element (FE) analysis was adopted by Tang et al. [9] to model a centrifuge test on the decrease of silty sand layer liquefaction potential by the use of stone column SC method. The silty sand layer's and SC's predicted responses were fairly close to the findings in the lab. Along with the shear stress distributions and shear stress drops, an examination was conducted of the total site-stiffening influences resulting from the installation of SCs. The impact of the surface load at the SC area and the hydraulic conductivity of SC on the liquefaction decrease activity was investigated using parametric research. The results demonstrated that the behavior of the SCs is in a combined shear and flexure mode. Furthermore, SCs with hydraulic conductivity above a certain threshold can significantly reduce the liquefaction risk.

By employing direct shear testing, Govind and Chandrakaran [10] investigated the increase in lateral load-carrying capability of soils reinforced with geosynthetic encased stone column in comparison to the soil supported by regular stone column. The findings demonstrated that the diameter of the stone shaft and the size of the stone utilized determine the shear stress and the angle of internal friction. It was discovered that when the regular stone column was swapped out for an encased stone column, there was an increase in shear stress and the angle of internal friction.

The impact of footing shape under cyclic stress circumstances on clay soil was examined by Najim et al. [11]. Square and circular locations with a defined footing area were the most common postures employed in the study. On cohesive soil with three undrained shear strengths (20 kPa, 40 kPa, and 70 kPa), cyclic load testing was carried out. In order to examine the effects of foundation depths on sediment change, total vertical stress, and two loading rates (3 mm / sec and 6 mm / sec), two depths were combined for the foundation: 5 cm and the surface. The transmitted total vertical stress increased as the loading rate of soft, medium clay increased, according to the results.

The current work is the second stage of the research conducted by Raheem et al. [12]. It aims to comprehend how soft soil reinforced with stone columns reacts to an earthquake load applied dynamically. Under various circumstances, geogrid-encased stone columns (GESC) and regular stone columns (OSC) were employed. In order to comprehend the strain mechanism, the current study focuses on the lateral dynamic response of foundations on soft soil under seismic stress (during vibration), the dynamic reaction of the stone column to lateral shaking, and the interaction of soil and structure.

2. Experimental Work

2.1 Soil used

Clayey soil was chosen from an area in Iraq south of the city of Baghdad. To ascertain the qualities of the soil, multiple laboratory studies have been conducted. Specific gravity in accordance with ASTM D854 [13] requirements, Atterberg limits (liquid and plastic limits) in accordance with ASTM D4318 [14], and grain size distribution (sieve analysis and hydrometer tests) in accordance with ASTM D422 [15] specifications are some of the studies that fall under above. According to the findings, the soil was made up of 22% silt, 75% clay, and 3% sand. The soil is categorized as CL type by the USCS. The soil's chemical and physical characteristics are presented in Table 1. Fig. 1 displays the grain size distribution of the clayey soil that was utilized.

Table 1: Clay soils' chemical and physical characteristics.

Properties	Account
(Liquid limit) %	44
(Plastic limit) %	22
(Plasticity index) %	22
(Specific gravity)	2.7
(Sand) %	3
(Silt) %	22
(Clay) %	75
(Maximum dry unit weight) kN/m^3	17.3
(Optimum moisture content) %	17
SO_3 %	0.58
Gypsum content %	1.24
pH	9.02
T.D.S.	1.69

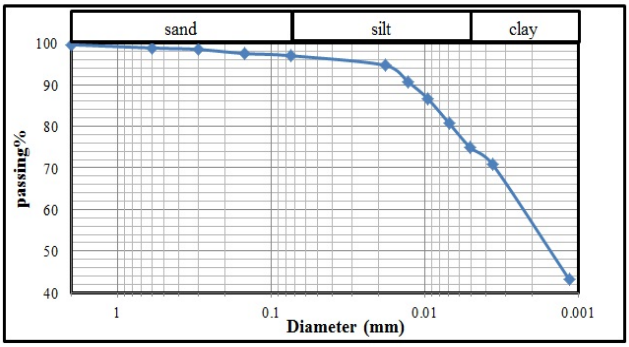

Fig. 1: Grain size distribution of the soil particles.

2.2 Broken stone

The broken stone came from a certain stone business that crushed big stones. The angular, white stone granules are shaped as such. In compliance with Al-Sheikhly's [16] recommendations, crushed stone with a grain size of approximately 1/7 to 1/9 of the stone columns' diameter was selected. The ASTM C128-04a [17] states that the specific gravity is 2.62, the dry unit weight is 15.5 kN/m^3, and the particle sizes range from 4 to 10 mm.

3. Preparation of Model Tests

3.1 Preparation of soil

The shear strength diversity of the clay soil must be measured against the time after mixing with various moisture contents before producing the soil layer in the container. As a result, six samples with various moisture concentrations were made separately. Every component is layered five times inside a CBR mold. To release the trapped air in each stratum, a different hammer was utilized. The samples were then sealed with polythene sheets and left for a period of seven days. Every day, the undrained shear strength was measured using a portable vane shear device. As seen in Fig. 2, these experiments allow the soil to rest for a while in order to regain strength following the mixing procedure. The time effect and soil shear strength both diminish with increasing water content. The shear resistance variance of the soil with water content over the next 72 hours is explained in Fig. 3.

The soil is placed in a container with an undrained shear strength of 15 kN/m2, or 30% water content, in accordance with the conclusion drawn from Figure 3. Additionally, the soil was prepared with an undrained shear strength of 25 kPa, which corresponds to the produced container's 28% water content. 500 kg of soil were divided into 20 kg groups for the soil preparation process; water was added to each group to achieve the desired consistency. For a full day, moist mixed soil is packed into plastic bags.

Subsequently, five dirt layers have been stacked inside an 800 x 800 x 1000 mm steel container; each layer is lightly pounded with a 50 x 100 mm wooden hammer. As recommended by Fattah et al. [18], the soil was allowed to recover its strength between 15 and 25 kPa over the course of three days.

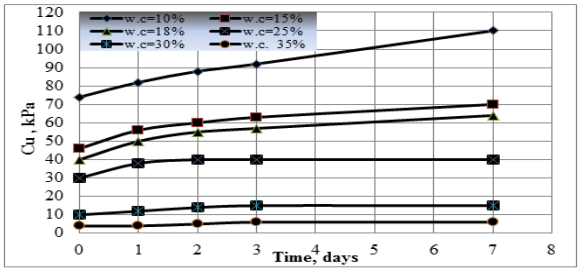

Fig. 2: Relationship of the undrained shear strength for time.

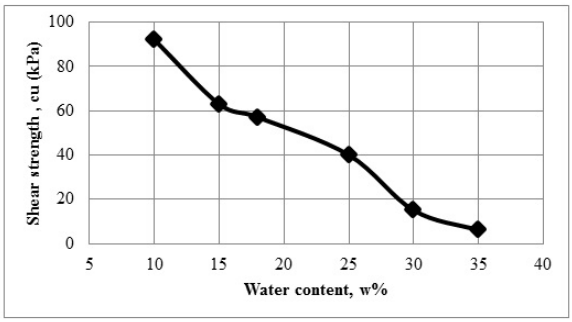

Fig. 3: Variation of the undrained shear strength with water content after 3- day curing.

3. 2 Composition of the stone columns

Following the preparation of the earth bed, the stone columns' construction process begins. The stone column's depth, with L = 400 mm and D = 50 mm, is equal to (L / D = 8). A particular depth was reached by pushing down the earth using a (50 mm) outside diameter (PVC) tube. The procedure for installing a stone column is depicted in Fig. 4. A (hand drill), made specifically for this purpose, is used to remove the soil from the inside of the tube. The PVC pipe was then carefully taken out. To achieve a density of 15.5 kN/m^3, the stone is placed in five layers, each of which is piled by a rod with a 44 mm diameter.

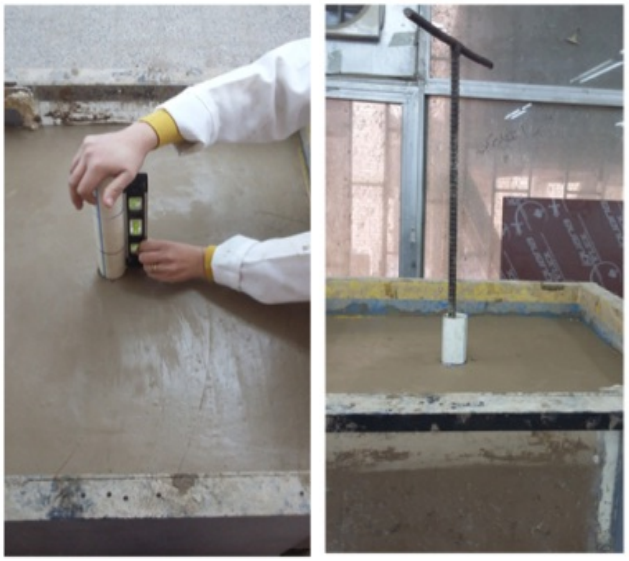

Fig. 4: The process of stone column installation.

3. 3 Composition of the (encased-stone column)

The process of creating geogrid pipes involves shaping and sewing the geogrid mesh roll using nylon threads along a coated stone column that has a diameter of 48 mm and a length of L/D = 8. After the earth layer was ready, the construction process for the stone column encased in geogrid started. There is a holy plastic tube that has an exterior diameter of 50 mm. One inserts the plastic tube into the ground. The soil inside the plastic tubes is removed using a manual auger. Next, a PVC tube is used to insert it

into the tube geogrid stone column hole. A rod is used to build each layer of stone to give the final product a dry unit weight of 15.5 kN/m^3. Fig. 5 displays the procedure of building the encased stone-column.

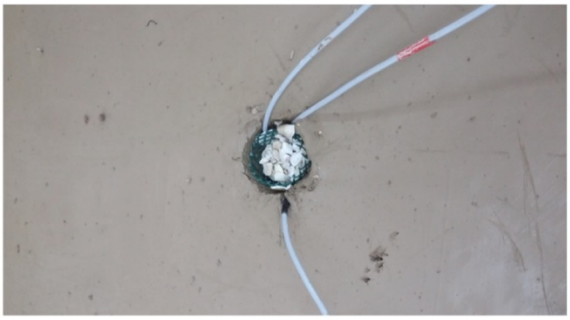

Fig. 5: Steps of geogrid encased stone column installation.

3.4 Application of loads on the footing

The theoretical ultimate bearing capacity of the footing was determined based on the following variables: depth of foundation, breadth of foundation, undrained shear strength, and shape of foundation. This allowed for the selection of the value of the imposed load on the footing model. Based on Hansen equation [19, 20] (Hansen, 1970; Bowles, 1996), the following calculations were performed for a soft clay soil with safety factor 3 and shear resistance (16) kPa:

$$q_{ult} = c.\ Nc\ .Sc.\ dc.\ ic.\ gc.\ bc + q.\ Nq.\ Sq.\ dq.\ iq.\ gq.\ bq + 0.5\ g.B.\ N\gamma.S\gamma.d\gamma.i\gamma.\ g\gamma.\ b\gamma \quad (1)$$

where:

q_{ult} = ultimate bearing capacity,

c = cohesion of soil,

q = surcharge (γ Df),

D_f = depth of the footing,

Nc, Nq and Nγ = bearing capacity factors,

B = width of foundation,

γ = soil unit weight,

Sc, Sq, Sγ = shape factors,

dc, dq, dγ = factors of depth,

ic , iq, iγ = factors of inclination,

gc , gq, gγ = factors of ground, and

bc , bq, bγ = factors of base.

For the soil used in this study, the value of (f) is equal to 0 (cohesive soil) so the above equation becomes:

$$q_{ult} = 5.14\ c_u\ (1 + s_c + d_c - i_c - b_c - g_c) + q \quad (2)$$

A square steel foundation is used for dimensions (0.75 mm x 0.75 mm) and 20 mm thickness in the center of the base area.

4. Design and Manufacturing of the Model (Model of Shaking Table)

Using a shaking table is one of the methods that may be used to replicate the excitation and loading of an earthquake in a lab setting. A vital piece of lab equipment for simulating loading during dynamic excitation, such as an earthquake, is the shaking table. There are various types of loadings, such as random, harmonic, and genuine seismic motion. One of the simplest and least expensive methods is the shaking table; it can replicate any kind of dynamic loading and be connected to any PC program or software.

In this study, dynamic motion of a harmonic form at various frequencies is the input motion produced by the shaking table. As seen in Fig. 6, the shaking table device is primarily composed of four parts:

- Shaking table base.
- Electrical motor and Ac-drive.
- Steel container.
- Damping system.

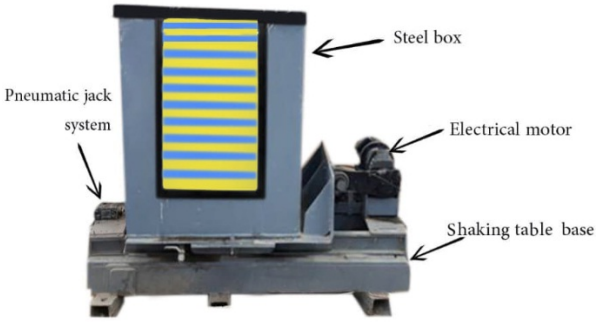

Fig. 6: Shaking table setup.

5. Steps Model Tests

Typical tests were conducted with a stone column on enhanced natural soil. For soft clay soils, a total of eighteen dynamic load test models comprising two series were conducted with varying shear strengths. To estimate the limits of the dynamic load of foundations in soft (untreated) soils susceptible to seismic stress (during vibrations), six models were tested. Three frequencies (0.5, 1 and 2 Hz) for the device were used to test the models. Similarly, twelve foundation models with three distinct frequency ranges (0.5, 1, and 2 Hz) of the apparatus were evaluated to treat soft soils under dynamic loads on regular and enclosed stone columns. The base is placed with dimensions (75 x 75 mm) on the surface of the soft soil model that has not been treated and the soil model that has been treated with regular and geogrid-encased columns. The maximum permitted static load on the footing initially loads the footing.

Using a time-off-light sensor (LVDT) under earthquake stress, the foundation's horizontal displacement has been measured (during shaking). It is feasible to think of the system as a tiny lidar system because flight sensor technology was utilized to precisely measure the amount of time it takes for pulses of infrared laser light to reach the closest object and be reflected back to the detector, as shown in Fig. 7.

Under seismic load (during vibrations), the horizontal stress of the regular and encased stone column was measured using the pressure cell sensors depicted in Figure 8. To directly monitor the pressure on the stone column wall, the incredibly flexible A201TEKSCAN flexible pressure sensors with a 1500 kPa flexi-force sensor capability were employed. Three pressure sensors were employed; as illustrated in Fig. 7, the first sensor was positioned one-third the depth of the stone column, the second one-third the length of the stone column on the opposite side of the first sensor, and the third one-half the length of the stone column below the first sensor. With pressure sensor measurements of 0.203 mm thick, 14 mm broad, and 9.53 mm in area, a comparatively high number of sensors could be installed from the wall due to their size and thickness.

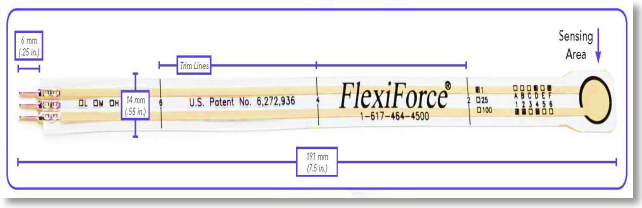

Fig. 7: Dimensions and shape of the sensor used.

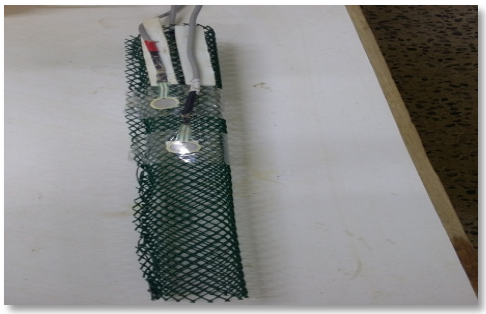

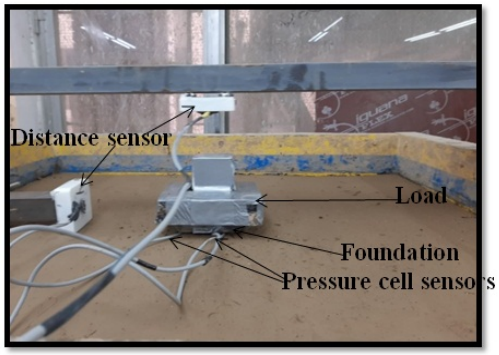

Fig. 8: Model testing procedure.

6. Results and Illustrations

The relationship between the horizontal stresses recorded at various soil column levels and time for footings on regular and encased stone columns built in soft clay with cu = 15 kPa and 25 kPa at various frequencies (0.5, 1 and 2 Hz) is depicted in Figs. 9 to 20.

Under varying frequencies and with cu = 15 and 25 kPa, the stress values at half the depth of the stone column are larger than those at the third depth of the stone column in both the ordinary and encased cases. Because of the shaking, the consequent pressure variation is visible along the typical stone column. At both the 15 and 25 kPa undrained shear strengths of soft clay, the stress values declined with frequency. However, in the instance of the encased stone column, the resulting pressure fluctuation grew in value at 15 kPa of undrained soft clay shear strength with increasing frequency. The values of the maximum horizontal stress along the stone column at two depths are recorded in Table 2.

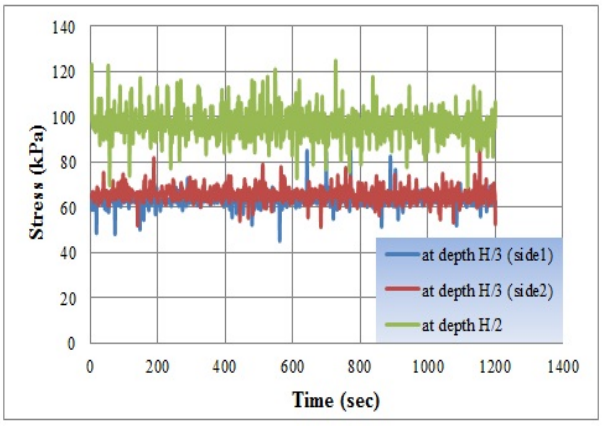

Fig. 9: Horizontal stresses – time relationship of model footing on ordinary stone column under 0.5 Hz frequency, cu= 15 kPa.

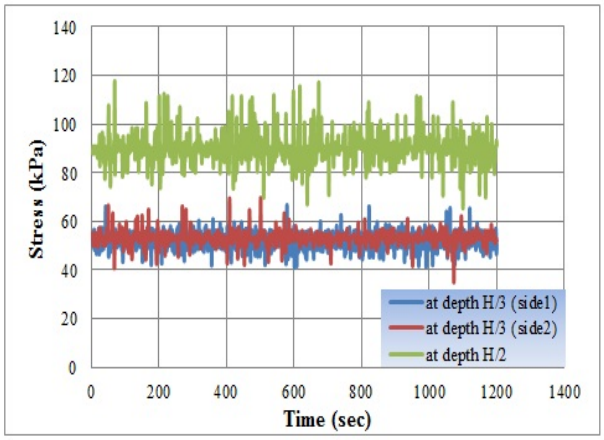

Fig. 10: Horizontal stresses – time relationship of model footing on ordinary stone column under 1 Hz frequency, cu= 15 kPa.

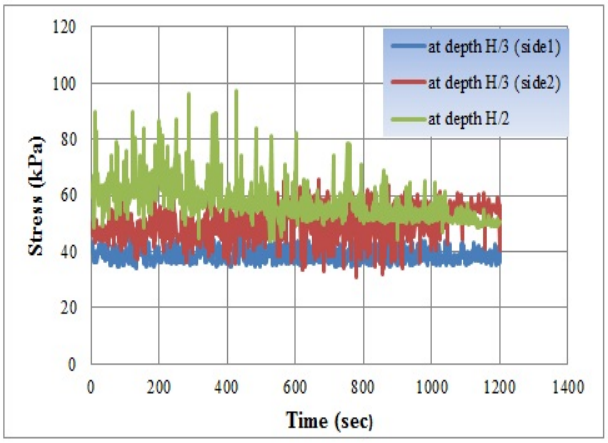

Fig. 11: Horizontal stresses – time relationship of model footing on ordinary stone column under 2 Hz frequency, cu= 15 kPa.

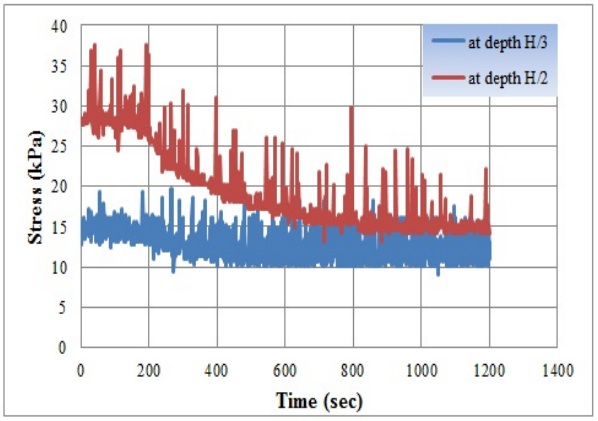

Figure 12. Horizontal stresses – time relationship of model footing on geogrid encased stone column under 0.5 Hz frequency, cu= 15 kPa.

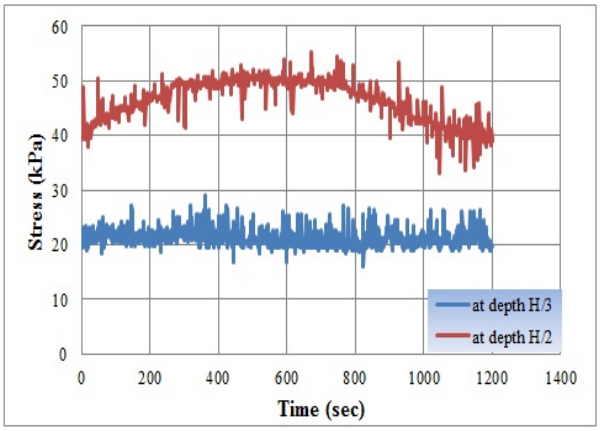

Fig. 13: Horizontal stresses – time relationship of model footing on geogrid encased stone column under 1 Hz frequency, cu= 15 kPa.

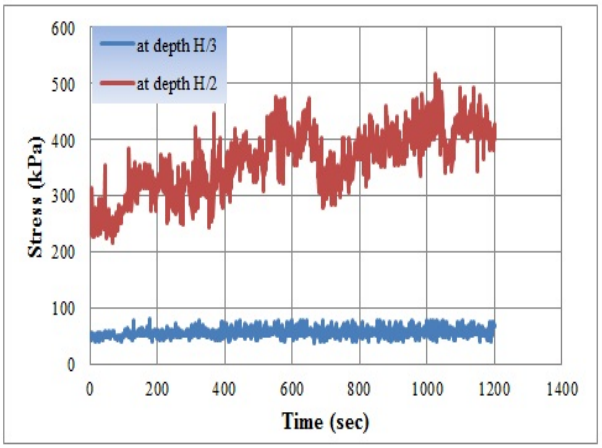

Fig. 14: Horizontal stresses – time relationship of model footing on geogrid encased stone column under 2 Hz frequency, cu= 15 kPa.

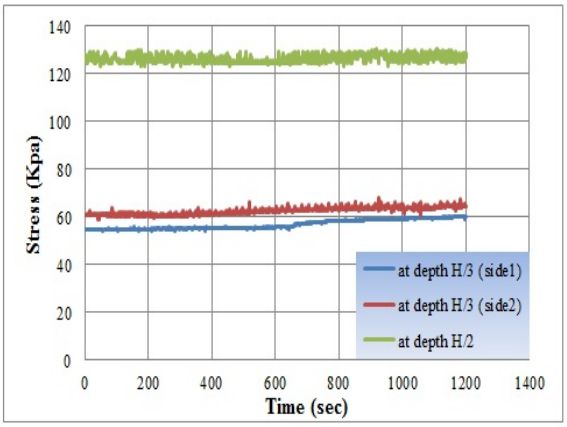

Fig. 15: Horizontal stresses – time relationship of model footing on ordinary stone column under 0.5 Hz frequency, cu= 25 kPa.

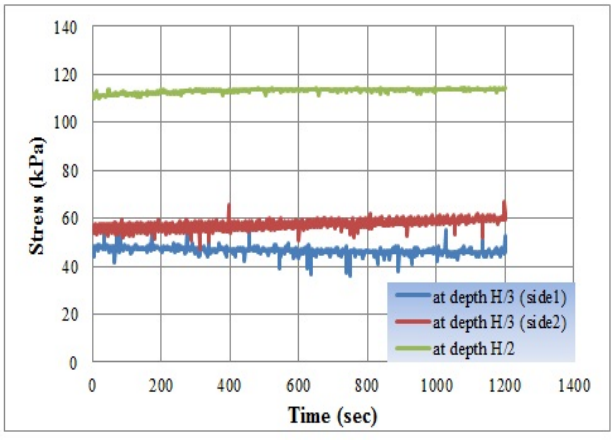

Fig. 16: Horizontal stresses – time relationship of model footing on ordinary stone column under 1 Hz frequency, cu= 25 kPa.

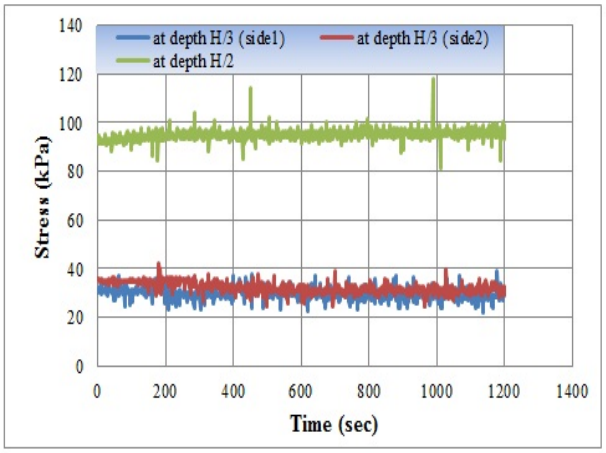

Fig. 17: Horizontal stresses – time relationship of model footing on ordinary stone column under 2 Hz frequency, cu= 25 kPa.

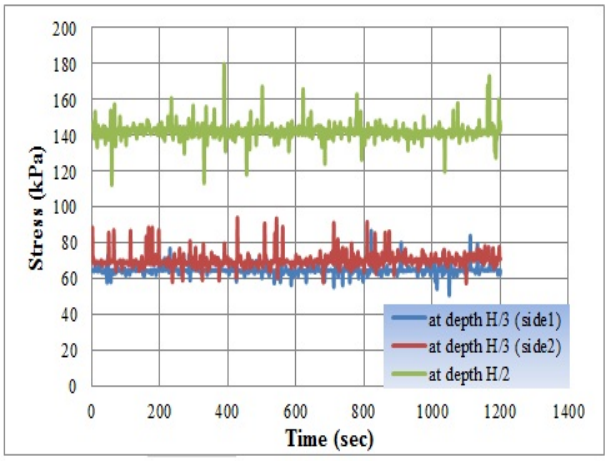

Fig. 18: Horizontal stresses – time relationship of model footing on geogrid encased stone column under 0.5 Hz frequency, cu= 25 kPa.

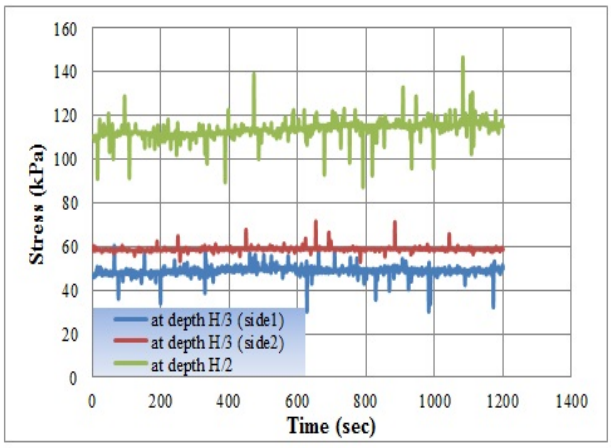

Fig. 19: Horizontal stresses – time relationship of model footing on geogrid encased stone column under 1 Hz frequency, cu= 25 kPa.

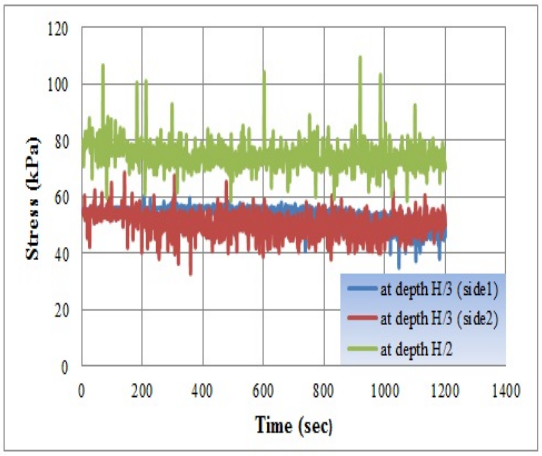

Fig. 20: Horizontal stresses – time relationship of model footing on geogrid encased stone column under 2 Hz frequency, cu= 25.

Returning to Figs. 9 to 20 and Table 2, we can see that when the frequency of the model footing on regular stone columns rises, the horizontal stresses in the soft clay with undrained shear strength (15 and 25) kPa decrease in value. For example, at a depth of one third the length of an average stone column, the amount of horizontal stress drops in proportion of (13.5) % when the frequency is increased from (0.5-1) Hz in the soil with a resistance amount of 15 kPa. Furthermore, the amount of horizontal tension reduces by roughly (39.9) % at the same depth when the frequency is increased from (0.5-2) Hz.

Furthermore, at a depth of half the length of an average stone column, the amount of horizontal stress reduces in proportion by (4.9) % when the frequency is increased from (0.5-1) Hz in the soil with a resistance amount of 15 kPa. Furthermore, the amount of horizontal tension reduces by about (27.1) % at the same depth when the frequency is increased from (0.5-2) Hz.

It is evident that when the clay soil's undrained shear strength was increased from 15 to - 25 kPa, the values of lateral stress reduced. For instance, the horizontal stress at a depth of 1/3H in the case of undrained shear strength 15 is approximately 21.5% more than the horizontal stress in the case of undrained shear strength 25 at a frequency of 0.5 Hz of model footing on regular stone columns. In certain experiments, raising the soil's strength from (15–25) kPa by around 5.9% of the model footing on regular stone columns results in an increase in the horizontal stress at a depth of 1/2H at a frequency of 0.5 Hz.

It is observed that the model on soil treated with a geogrid-encased stone column has a higher value of horizontal stress than the model on soil treated with an ordinary stone column. In certain experiments, the model for soil treated with a regular stone column exhibits higher values of horizontal stresses than the model for soil treated with a stone column encased in geogrid. For instance, at a depth of

1/3H, the horizontal stress values in the model footing on soil treated with OSC reduce by approximately 74.9% compared to the model on soil treated with GESC at a frequency of 0.5 Hz and an undrained shear strength of 15k Pa. The horizontal stress readings for the GESC treated soil model are approximately (21.6%) higher than the OSC treated soil model at a depth of 1/3 h at 2 Hz and an undrained shear strength of 15 kPa. Stated otherwise, when the soil treated with OSC experiences an increase in frequency, the horizontal frequency falls, and when the soil treated with GESC experiences an increase in frequency at a depth of 1/3 hour, the horizontal frequency increases.

Table 2: Maximum horizontal stresses of the model footings at varied frequencies and undrained shear strengths of soft clay handled with regular and enclosed stone columns.

Undrained shear strength (cu), kPa	Depth	Max horizontal stress (kPa)					
		Soil type					
		Ordinary stone-column			Geogrid encased stone-column		
		Frequency, Hz					
		0.5	1	2	0.5	1	2
15	H/3	76.53	66.21	45.96	------	------	-----
	H/3	78.63	69.70	61.88	19.76	27.16	78.91
	H/2	123.09	117.11	89.75	37.61	54.59	506.85
25	H/3	60.09	55.69	37.35	84.00	60.36	60.46
	H/3	66.52	65.62	42.28	91.69	71.48	68.66
	H/2	130.74	114.49	100.94	179.85	146.59	109.43

7. Conclusions

1. Model footings on clay treated with ordinary stone columns fail only under 2 Hz frequency while no failure was recorded for model footings on clay treated with geogrid encased stone columns.

2. Under various frequencies, in both the conventional and encased cases, and with cu = 15 and 25 kPa, the stress values at half the depth of the stone column are larger than those at its third.

3. By raising the clay soil's undrained shear strength from 15 to 25 kPa, the values of lateral stress on the stone column dropped.

4. Compared to the model on soil treated with a stone column encased in geogrid, the horizontal stress is smaller in the soil treated with the regular stone column.

References

[1] Malarvizhi, SN, & Ilamparuthi, K (2004) Load versus settlement of clay bed stabilized with stone and reinforced stone columns. In 3rd Asian Regional Conference on Geosynthetics, pp. 322-329.

[2] Matsui, T, Ito, T, & Ohara, H (1980) Cyclic stress-strain history and shear characteristics of clay. Journal of the Geotechnical Engineering Division, ASCE, 106(10), 1101-1120.

[3] Procter, DC, & Khaffaf, JH (1984) Weakening of undrained saturated clays under cyclic loading. Journal of Geotechnical Engineering, ASCE, 110(10), 1431-1445.

[4] Munfakh, GA, Sarkar, SK, & Castelli, RJ (1984) Performance of a test embankment founded on stone columns. In Piling and ground treatment, pp. 259-265, Thomas Telford Publishing.

[5] Van Impe, WF, De Cock, F, Van Der Cruyssen, JP, & Maertens, J (1997) Soil improvement experiences in Belgium: part III. Case histories. Proceedings of the Institution of Civil Engineers-Ground Improvement, 1(4), 179-191.

[6] Adalier, K & Elgamal, A (2004) Mitigation of liquefaction and associated ground deformations by stone columns. Engineering Geology, 72(3-4), 275-291. DOI: 10.1016/j.enggeo.2003.11.001.

[7] Mok, YJ, Kim, HS & Park, CS (2015) S-wave cross-hole logging for stone columns. KSCE Journal of Civil Engineering 19, 911–916. https://doi.org/10.1007/s12205-013-0699-9.

[8] Ashour, S (2016) The response of stone columns under the cyclic loading, Doctoral dissertation, University of Birmingham, UK.

[9] Tang, L, Zhang, X & Ling, X (2016) Numerical simulation of centrifuge experiments on liquefaction mitigation of silty soils using stone columns. KSCE Journal of Civil Engineering 20, 631–638. https://doi.org/10.1007/s12205-015-0363-7.

[10] Govind, G and Chandrakaran, S (2017) Lateral load carrying capacity of soil reinforced with geosynthetic encased stone column, National Conference on Recent Advancements in Geotechnical Engineering, 28th March 2017, GCT, Coimbatore.

[11] Najim, AN, Fattah, MY, & Al-Recaby, MK (2020) Cyclic settlement of footings of different shapes resting on clayey soil. Engineering and Technology Journal, 38(3A), 465-477.

[12] Raheem, AM, Fattah, MY, & Al-Recaby, MK (2021) Earthquake Response of Model Footings on Soft Clays Strengthened by Stone Columns. Engineering and Technology Journal, 39 (08), 1216-1223.

[13] ASTM, D854 (2003) Standard Test Method for Specific Gravity of Soil Solids by Water Pycnometer, Soil and Rock (I), Vol. 04.08.

[14] ASTM, D4318 (2003) Standard Test Method for Liquid Limit, Plastic Limit, and Plasticity Index of Soils, Soil and Rock (I), Vol. 04.08.

[15] ASTM, D422 (2003) Standard Test Method for Particle-Size Analysis of Soils, Soil and Rock (I), Vol. 04.08.18.

[16] Al-Sheikhly, AA (2000), Effect of stone grain size on

the behavior of stone column, M.Sc. Thesis, Building and Construction Engineering Department, University of Technology, Iraq.

[17] ASTM C128-04a Standard Test Method for Density, Relative Density (Specific Gravity), and absorption of Fine Aggregate, USA.

[18] Fattah, MY, Shlash, KT, Al-Waily, MJ (2013) Experimental Evaluation of Stress Concentration Ratio of Model Stone Columns Strengthened by Additives, International Journal of Physical Modelling in Geotechnics, ICE, Vol. 13, No. (3), pp. 79–98, http://dx.doi.org/10.1680/ijpmg.12.00006.

[19] Hansen, JB (1970) A Revised and extended formula for bearing capacity, Bulletin of Danish Geotechnical Institutes, Vol. 28, pp. 5 – 11.

[20] Bowels, JE, (1996) Foundation analysis and design", 5th Edition, McGraw-Hill Book Company, P. 1175.

[21] Al-Recaby, MKM (2016) Dynamic response to lateral excitation of pile group in sandy soil, Ph.D. thesis, Building and Construction Engineering Department, University of Technology, Iraq.